INVARIANT SUBPIXEL MATERIAL IDENTIFICATION IN AVIRIS IMAGERY

Bea Thai, Glenn Healey, David Slater*

Abstract

We present an algorithm for subpixel material identification that is invariant to the illumination and atmospheric conditions. The target material spectral reflectance is the only prior information required by the algorithm. A target material subspace model is constructed from the reflectance using an image formation model and a background subspace model is estimated directly from the image. These two subspace models are used to compute maximum likelihood estimates for the target material component and the background component at each image pixel. These estimates form the basis of a generalized likelihood ratio test for subpixel material identification. We present experimental results using AVIRIS imagery that demonstrate the utility of the algorithm for subpixel material identification under varying illumination and atmospheric conditions.

1 Introduction

The recent development of airborne imaging spectrometers represents a major advance in remote sensing capability. For example, the Airborne Visible InfraRed Imaging Spectrometer (AVIRIS) sensor [11] acquires over 200 spatially registered images, taken over the spectral range 0.4μm-2.5μm. The sensor operates at approximately 20km above sea level. Each image pixel therefore covers an approximately 20m $\times$ 20m area. Often, the observed spectrum of a pixel is a mixture of spectra from several different materials within the spatial coverage of the pixel. The problem of subpixel detection requires identifying which pixels in an image contain a specified material. Since at subpixel scale, it is not possible to detect the material spatially, we must rely on spectral information. Fortunately, many materials exhibit characteristic spectral features that can be exploited for recognition [2].

A mixed pixel is a pixel that contains more than one material. Both linear and nonlinear models have been proposed to describe mixed pixels. In a linear model, a mixed pixel is represented as a linear combination of component or endmember spectra [6]. Since Johnson et al. [5] showed that nonlinear mixing [3] can be "linearized," recent research efforts have focused on developing detection algorithms using a linear model [1] [4] [7].

Many subpixel detection algorithms [1] [4] assume that the component spectra are known *a priori*. However, this prior knowledge is often difficult to obtain. Alternatively, appropriate spectral prototypes can be selected from an image to serve as component spectra [7]. It is usually difficult, however, to select

*The authors are with the Computer Vision Laboratory, Department of Electrical and Computer Engineering, University of California, Irvine, CA 92697. Email: bthai,healey,dslater@ece.uci.edu.

a single spectral prototype for a material since sensor spectral radiance is affected by atmospheric and geometric conditions that can vary spatially and temporally.

In this paper, we present an algorithm for subpixel detection in hyperspectral images. No prior information about the component spectra is assumed. The input to the algorithm is the spectral reflectance function of the material to be identified. Our approach is based on the use of linear subspaces to model the component spectra. We consider each pixel as a sum of two vectors, one from the target subspace [9] and the other from the background subspace. The target subspace contains material information over atmospheric and geometric conditions. The background subspace is estimated from the image.

2 Image Modeling

2.1 Linear Spectral Mixing

In a linear spectral mixing model, a mixed pixel is represented as a linear combination of component spectra. Let l denote the number of spectral bands and let $\boldsymbol{t}$ and β denote the target material spectrum and the fraction of target material. A mixed pixel, denoted by an l-dimensional vector $\boldsymbol{y}$, can be described by

$$\boldsymbol{y} = \beta \boldsymbol{t} + \sum_{i=1}^{m} \alpha_i \boldsymbol{e}_i + \boldsymbol{n} \tag{1}$$

where m is the number of background component spectra, $\boldsymbol{e}_i$ and α_i are the ith component spectrum and the fraction of the ith component spectrum, and $\boldsymbol{n}$ is an l-dimensional noise vector. The subpixel detection problem is to determine the presence or absence of the target signal $\beta \boldsymbol{t}$. Our approach is based on the use of linear subspaces. We assume that the background spectra span some subspace of the real vector space $\Re^l$ and that the target material spectrum lies in a different subspace within $\Re^l$.

2.2 Target Subspace

Targets are often modeled using a single spectrum. However, since the sensor spectral radiance for a material is affected by the atmospheric and geometric conditions, a target spectral signature can have significant variability. A more general method is to utilize a target subspace that accounts for atmospheric and geometric variation. Slater and Healey [9] showed that the set of sensor spectral radiance functions for a material can be well approximated by a small number of basis functions. We will use the basis functions generated using this approach to define a target subspace. Let $\boldsymbol{T}$ be an $l \times s$ matrix containing the orthonormal basis vectors that span the target subspace. Because this target subspace contains material information over atmospheric and geometric conditions, the same target subspace can be applied to any image that may contain the target.

2.3 Background Subspace

In this subsection, we describe a method for determining the background subspace from an image. Consider an image region of size $p \times q$ with l spectral bands. We construct a matrix $\boldsymbol{Y}$ of size $l \times pq$, where each column contains a hyperspectral pixel in the region and $pq \geq l$. The dimensionality of $\boldsymbol{Y}$ can be reduced using the singular value decomposition [10]

$$\boldsymbol{Y} = \boldsymbol{U}\boldsymbol{D}\boldsymbol{V}^T \tag{2}$$

where the columns of $\boldsymbol{U}$ are the eigenvectors of $\boldsymbol{Y}\boldsymbol{Y}^T$, the columns of $\boldsymbol{V}$ are the eigenvectors of $\boldsymbol{Y}^T\boldsymbol{Y}$, and the diagonal matrix $\boldsymbol{D}$ contains the singular values. If $\boldsymbol{y}_i$ denotes column i of $\boldsymbol{Y}$ and $\boldsymbol{u}_i$ denotes column i of $\boldsymbol{U}$, then each pixel $\boldsymbol{y}_i$ can be approximated by

$$\widehat{\boldsymbol{y}}_i = \sum_{j=1}^{r} (\boldsymbol{y}_i^T \boldsymbol{u}_j)\boldsymbol{u}_j \tag{3}$$

where $r < l$ is the reduced dimensionality. Let σ_j denote the jth singular value. For a given r, the squared error

$$\epsilon_r = \sum_{i=1}^{pq} ||\boldsymbol{y}_i - \widehat{\boldsymbol{y}}_i||^2 = \sum_{j=r+1}^{l} \sigma_j^2 \tag{4}$$

is minimized by selecting the $\boldsymbol{u}_j$ with the r largest singular values. We will assume that the singular values are sorted in descending order.

The first M background basis vectors $\boldsymbol{u}_j, 1 \leq j \leq M$, will always be included in the background subspace to ensure that the squared error is less than a fraction, t_M, of the total variance. The parameter M is set to the smallest integer such that

$$\epsilon_M \leq t_M \sum_{j=1}^{l} \sigma_j^2 \tag{5}$$

It is generally not advantageous to include too many basis vectors in the background subspace. The reason for this is that each background vector that is not orthogonal to the target subspace increases the overlap between the target and background subspaces. For this reason, a maximum of N basis vectors are used, $N \geq M$, where the parameter N is the smallest integer such that

$$\epsilon_N \leq t_N \sum_{j=1}^{l} \sigma_j^2 \tag{6}$$

for a threshold t_N. We include selectively background basis vectors in the range $\boldsymbol{u}_{M+1}, \ldots, \boldsymbol{u}_N$ that are not similar to the target subspace. We define the similarity of a background basis vector $\boldsymbol{u}_j$ to the target subspace $\boldsymbol{T}$ by the length of its projection onto $\boldsymbol{T}$

$$\delta_j = ||\boldsymbol{T}^T \boldsymbol{u}_j|| \tag{7}$$

If $\boldsymbol{u}_j$ is orthogonal to $\boldsymbol{T}$, then $\delta_j = 0$. We include $\boldsymbol{u}_j$ in the background subspace if δ_j is less than a threshold, t_δ. Therefore, the background subspace matrix $\boldsymbol{B}$ of size $l \times r$, where $M \leq r \leq N$, is given by

$$\boldsymbol{B} = \left[\begin{array}{cccccc} \boldsymbol{b}_1 & \cdots & \boldsymbol{b}_M & \boldsymbol{b}_{M+1} & \cdots & \boldsymbol{b}_r \end{array} \right]$$

where for $1 \leq j \leq M$, $\boldsymbol{b}_j = \boldsymbol{u}_j$ and for $M+1 \leq j \leq r$, the $\boldsymbol{b}_j$ are selected from the set $\{\boldsymbol{u}_{M+1}, \ldots, \boldsymbol{u}_N\}$ such that $\delta_j \leq t_\delta$.

3 Invariant Subpixel Detection

3.1 Maximum Likelihood Estimation

We assume that the columns of $\boldsymbol{B}$ and $\boldsymbol{T}$ are linearly independent and that $r + s < l$. Let $\boldsymbol{A} = [\boldsymbol{B}, \boldsymbol{T}]$ denote the matrix formed by concatenating matrices $\boldsymbol{B}$ and $\boldsymbol{T}$ in that order. A pixel $\boldsymbol{y}$ can be described

by

$$\boldsymbol{y} = \boldsymbol{B}\boldsymbol{\phi} + \boldsymbol{T}\boldsymbol{\theta} + \boldsymbol{n} = \boldsymbol{A}\begin{bmatrix} \boldsymbol{\phi} \\ \boldsymbol{\theta} \end{bmatrix} + \boldsymbol{n} \tag{8}$$

where $\boldsymbol{\phi}$ and $\boldsymbol{\theta}$ are r-dimensional and s-dimensional parameter vectors. Thus, $\boldsymbol{B}\boldsymbol{\phi}$ and $\boldsymbol{T}\boldsymbol{\theta}$ each specifies a particular vector in the respective subspaces. If $\boldsymbol{n}$ consists of statistically independent, identically distributed Gaussian random variables, then the least squares estimates of the parameters are the same as the maximum likelihood estimates. The least squares estimates for the parameters $\boldsymbol{\phi}$ and $\boldsymbol{\theta}$, denoted by $\widehat{\boldsymbol{\phi}}$ and $\widehat{\boldsymbol{\theta}}$, are given by

$$\begin{bmatrix} \widehat{\boldsymbol{\phi}} \\ \widehat{\boldsymbol{\theta}} \end{bmatrix} = \boldsymbol{A}^{+}\boldsymbol{y} \tag{9}$$

where $\boldsymbol{A}^{+}$ is the pseudoinverse of $\boldsymbol{A}$. The estimation of the parameter vectors is simplified if $\boldsymbol{A}$ is transformed into a matrix $\boldsymbol{Q}$ with orthonormal columns using the Gram-Schmidt process. Then,

$$\begin{aligned} \boldsymbol{B}\widehat{\boldsymbol{\phi}} + \boldsymbol{T}\widehat{\boldsymbol{\theta}} &= \boldsymbol{A}\boldsymbol{A}^{+}\boldsymbol{y} \\ &= \boldsymbol{Q}\boldsymbol{Q}^{T}\boldsymbol{y} \end{aligned} \tag{10}$$

3.2 Generalized Likelihood Ratio

We pose the detection problem as a hypothesis test between the hypotheses

$$\begin{aligned} H_0 &: \quad \boldsymbol{y} = \boldsymbol{B}\boldsymbol{\phi} + \boldsymbol{n} \\ H_1 &: \quad \boldsymbol{y} = \boldsymbol{B}\boldsymbol{\phi} + \boldsymbol{T}\boldsymbol{\theta} + \boldsymbol{n} \end{aligned}$$

where $\boldsymbol{\phi}$ and $\boldsymbol{\theta}$ are unknown parameter vectors and $\boldsymbol{n}$ is a zero mean Gaussian random vector with covariance $\boldsymbol{\Sigma}$. The decision rule that determines which hypothesis produced the data is the likelihood ratio

$$\Lambda(\boldsymbol{y}) = \frac{p_1(\boldsymbol{y}/H_1)}{p_0(\boldsymbol{y}/H_0)} \tag{11}$$

where $p_i(\boldsymbol{y}/H_i)$ is the conditional probability density of the observed $\boldsymbol{y}$ given that hypothesis H_i is true. Under hypothesis H_0, $\boldsymbol{y}$ is Gaussian distributed with mean $\boldsymbol{B}\boldsymbol{\phi}$ and covariance $\boldsymbol{\Sigma}$, or $p_0(\boldsymbol{y}/H_0) = \mathcal{N}(\boldsymbol{B}\boldsymbol{\phi}, \boldsymbol{\Sigma})$. Under hypothesis H_1, $p_1(\boldsymbol{y}/H_1) = \mathcal{N}(\boldsymbol{B}\boldsymbol{\phi} + \boldsymbol{T}\boldsymbol{\theta}, \boldsymbol{\Sigma})$. The generalized likelihood ratio is obtained when the unknown parameters are replaced by their maximum likelihood estimates. The parameters are estimated separately for each hypothesis.

3.3 Noise Estimation

For the experiments reported in this paper, we assumed that $\boldsymbol{\Sigma} = \sigma^2\boldsymbol{I}$. In future work, we will examine the use of more general noise models. For an l-dimensional Gaussian random vector with covariance $\sigma^2\boldsymbol{I}$, the maximum likelihood estimate of σ^2 under hypothesis i is given by [8]

$$\widehat{\sigma}_i^2 = \frac{||\boldsymbol{y} - \widehat{\boldsymbol{m}}_i||^2}{l} \tag{12}$$

where $||\cdot||$ denotes the vector length and $\widehat{\boldsymbol{m}}_i$ is the maximum likelihood estimate of the mean under hypothesis i. Substituting (12) into (11) and then raising to the $\frac{2}{l}$ power yields the generalized likelihood ratio

$$\widetilde{\Lambda}(\boldsymbol{y}) = (\Lambda(\boldsymbol{y}))^{\frac{2}{l}} = \frac{||\boldsymbol{y} - \widehat{\boldsymbol{m}}_0||^2}{||\boldsymbol{y} - \widehat{\boldsymbol{m}}_1||^2} \tag{13}$$

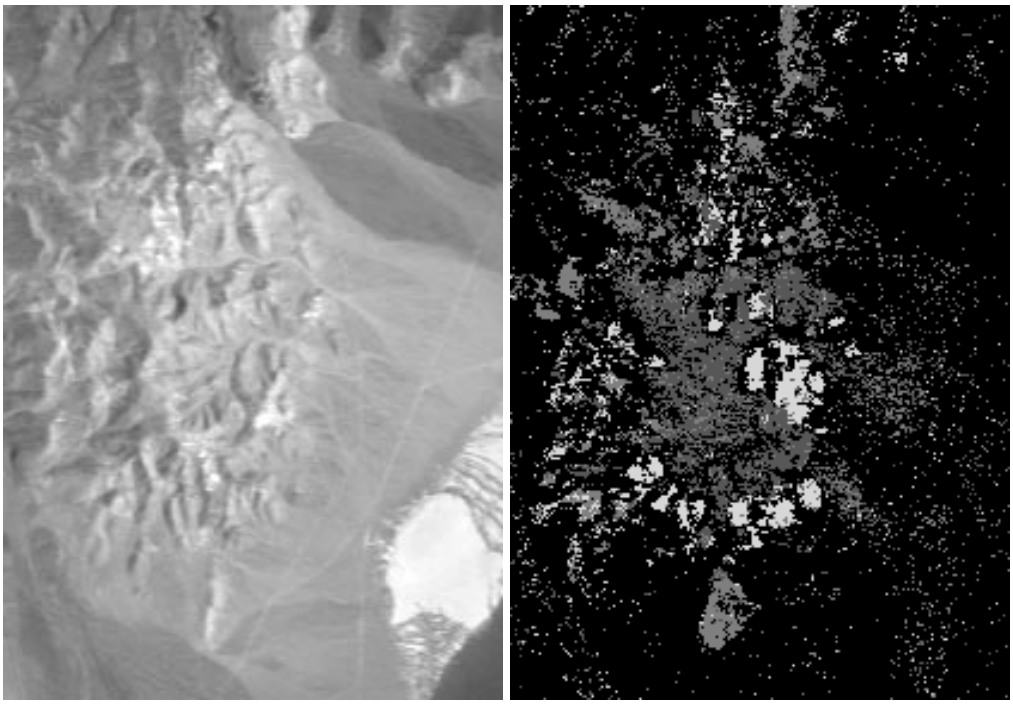

(a) (b)

Figure 1: Cuprite mining district: (a) band 120, (b) labeled mineral pixels

Since the maximum likelihood estimate of the mean is also the least squares estimate of the mean, $\widehat{\boldsymbol{m}}_0 = \boldsymbol{B}\boldsymbol{B}^T\boldsymbol{y}$ and $\widehat{\boldsymbol{m}}_1$ is given by (10). The generalized likelihood ratio is therefore given by

$$\tilde{\Lambda}(\boldsymbol{y}) = \frac{\boldsymbol{y}^T(\boldsymbol{I} - \boldsymbol{B}\boldsymbol{B}^T)\boldsymbol{y}}{\boldsymbol{y}^T(\boldsymbol{I} - \boldsymbol{Q}\boldsymbol{Q}^T)\boldsymbol{y}} \tag{14}$$

The larger the ratio is, the more likely that the pixel contains the target material. We can also interpret (14) as the ratio of fitting errors.

4 Experimental Results

We verified the subpixel detection algorithm presented in this paper using AVIRIS imagery. Figure 1(a) shows a region of the mining district in Cuprite, Nevada. This AVIRIS image was acquired in May 1994. The size of this image is approximately 200×300 pixels. In this experiment, we considered 3 minerals having the sample spectral reflectance plotted in figures 2 through 4. These reflectance functions were obtained from the USGS Digital Spectral Library (http://speclab.cr.usgs.gov/spectral-lib.html).

For this experiment, we used spectra from the image to build a set of basis functions for each of the minerals. Because mineral spectral variability is limited in this region of the image, $s = 2$ basis functions were sufficient to represent the target subspace. We computed the background subspace as described in section 2.3. There are three parameters in the background model: t_M and t_N that determine the minimum and maximum numbers of background basis vectors, and t_δ that determines the allowable

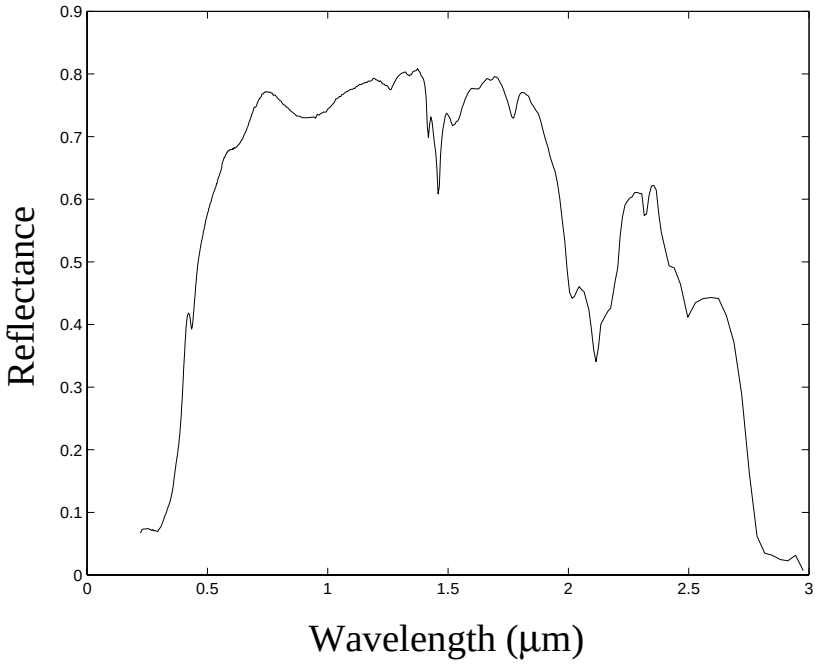

Figure 2: Sample reflectance function for a mixture of alunite/silica

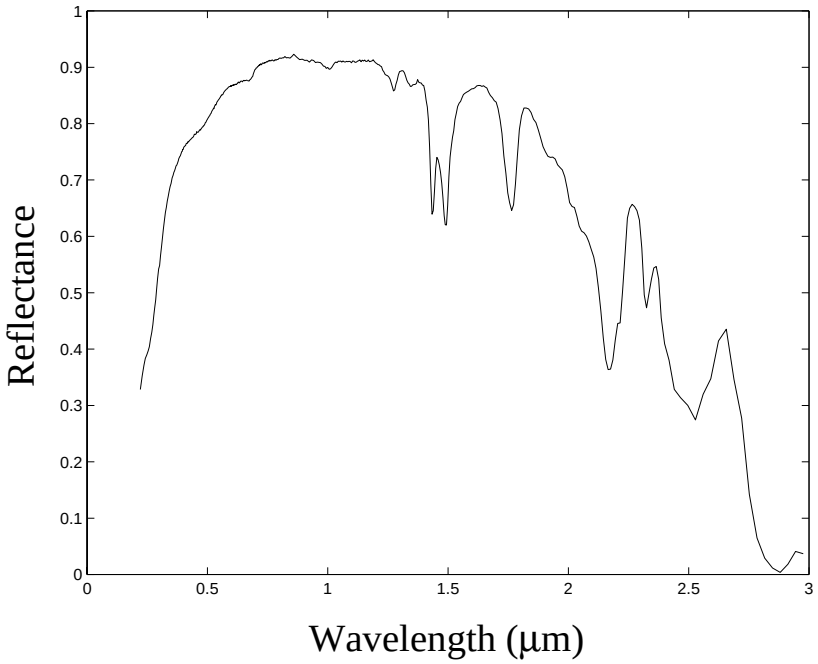

Figure 3: Sample reflectance function for alunite

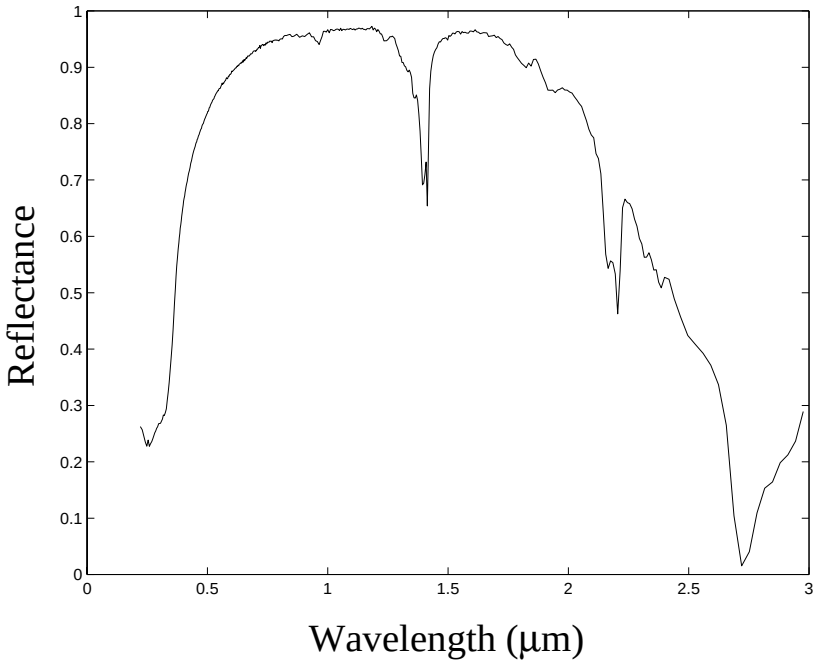

Figure 4: Sample reflectance function for kaolinite

overlap between a basis vector and $\boldsymbol{T}$. For this image, we set $t_M = t_N = 3.69 \times 10^{-5}$. Because $t_M = t_N$, the parameter t_δ is irrelevant. For each mineral, we obtained a likelihood map by computing the likelihood ratio according to (14) for each pixel in the region. A pixel is classified as belonging to the mineral that has the highest likelihood ratio among the 3 likelihood values. The classification results are shown in figure 1(b). The white pixels are alunite, the light gray pixels are kaolinite, and the dark gray pixels are a mixture of alunite and silica.

5 Summary

We have presented an algorithm for subpixel material identification that is invariant to the illumination and atmospheric conditions. We consider each pixel as a sum of two vectors, one from the target subspace and the other from the background subspace. For each image region, we compute a basis that represents the background subspace. The target subspace is computed from the spectral reflectance function and contains material information over atmospheric and geometric conditions. We have included experimental results using AVIRIS imagery that demonstrate the utility of the algorithm for subpixel material identification.

Acknowledgment

This research has been supported in part by the Air Force Office of Scientific Research, the Air Force Research Laboratory, and the Defense Advanced Research Projects Agency under grant F49620-97-1-0492.

References

[1] J. Adams, M. Smith, and P. Johnson. Spectral mixture modeling: A new analysis of rock and soil types at the Viking Lander 1 site. *J. Geophys. Res.*, 91(B8):8098–8112, July 1986.

[2] A. Goetz, G. Vane, J. Solomon, and B. Rock. Imaging spectrometry for earth remote sensing. *Science*, 228(4704):1147–1153, June 1985.

[3] B. Hapke. Bidirectional reflectance spectroscopy. I. Theory. *J. Geophys. Res.*, 86(B4):3039–3054, Apr. 1981.

[4] J. Harsanyi and C. Chang. Hyperspectral image classification and dimensionality reduction: An orthogonal subspace projection approach. *IEEE Trans. on Geosci. Remote Sensing*, 32(4):779–785, July 1994.

[5] P. Johnson, M. Smith, S. Taylor-George, and J. Adams. A semiempirical method for analysis of the reflectance spectra of binary mineral mixtures. *J. Geophys. Res.*, 88(B4):3557–3561, Apr. 1983.

[6] D. Nash and J. Conel. Spectral reflectance systematics for mixtures of powdered hypersthene, labradorite, and ilmenite. *J. Geophys. Res.*, 79(11):1615–1621, Apr. 1974.

[7] T. Nichols, J. Thomas, W. Kober, and V. Velten. Interference-invariant target detection in hyperspectral images. In S. Shen and M. Descour, editors, *Algorithms for Multispectral and Hyperspectral Imagery IV*, Proc. SPIE Vol. 3372, pages 176–187, Apr. 1998.

[8] L. Scharf and B. Friedlander. Matched subspace detectors. *IEEE Trans. Signal Processing*, 42(8):2146–2157, Aug. 1994.

[9] D. Slater and G. Healey. Exploiting an atmospheric model for automated invariant material identification in hyperspectral imagery. In S. Shen and M. Descour, editors, *Algorithms for Multispectral and Hyperspectral Imagery IV*, Proc. SPIE Vol. 3372, pages 60–71, Apr. 1998.

[10] G. Strang. *Linear Algebra and its Applications*. Harcourt Brace Jovanovich, Inc., San Diego, 3rd edition, 1988.

[11] G. Vane et al. The Airborne Visible/Infrared Imaging Spectrometer (AVIRIS). *Remote Sensing of Environment*, 44:127–143, May-June 1993.